



Comparative study on WRF model simulations from the viewpoint of optimum ship routing

Chen, Chen
Sasa, Kenji
Ohsawa, Teruo
Prpic-Orsic, Jasna

(Citation)

Ocean Engineering, 207:107379-107379

(Issue Date)

2020-07-01

(Resource Type)

journal article

(Version)

Version of Record

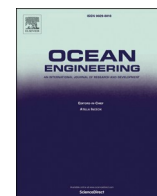
(Rights)

© 2020 The Authors. Published by Elsevier Ltd.
This is an open access article under the CC BY-NC-ND license
(<http://creativecommons.org/licenses/by-nc-nd/4.0/>).

(URL)

<https://hdl.handle.net/20.500.14094/90007199>





Comparative study on WRF model simulations from the viewpoint of optimum ship routing

Chen Chen^{a,*}, Kenji Sasa^a, Teruo Ohsawa^a, Jasna Prpić-Oršić^b

^a Department of Maritime Sciences, Kobe University, Kobe, Japan

^b Faculty of Engineering, University of Rijeka, Rijeka, Croatia

ARTICLE INFO

Keywords:

WRF regional Model
Physics parametrization schemes
GPV datasets
Gridded nudging
Rough-sea navigation
Ship weather routing

ABSTRACT

In addition to other studies focused on the WRF performance of rainfall, temperature, and precipitation, the present study provides practical suggestions for ship operators on choosing grid point value (GPV) datasets and WRF modeling approaches to help make better decisions on weather routing by estimating strong wind with a higher accuracy. Two different GPV datasets, the NCEP-FNL and ERA-Interim, are used for WRF modeling. Various modeling approaches, which include applying different physics options and choosing whether to adopt the four-dimensional-data-assimilation, are employed for numerical simulation. Then, on-board measurements of a bulk carrier has been used to validate the calculated wind of eight rough-sea navigational cases. This occurs over a wide spatial range, covering ocean regions such as the Northwest Pacific Ocean, South of Australia, Tasman Sea, Southeast of Africa, and Southeast of America, as well as a wide temporal range of four years. Results of 64 WRF simulations show that ERA-Interim is suitable for longer periods, while NCEP-FNL can analyze extremely high winds. Additionally, grid nudging can also reduce the wind strength due to its smoothing effect. Finally, selections of these different GPV datasets and modeling approaches for ship weather routing are discussed, particularly for rough-sea navigations.

1. Introduction

The Weather Research and Forecasting (WRF) model has been widely used with terrain following mass coordinates and the 3rd order Runge-Kutta integration scheme (Skamarock and Klemp, 2008) as a next-generation mesoscale numerical weather prediction model for operational forecasting and atmospheric research (Jianfeng, G. U., et al., 2005; Davis et al., 2008; Cha and Wang, 2013). This demonstrates the high capability and flexibility of the WRF model to elucidate various atmospheric phenomena in different regions. However, due to the chaotic nature of the atmosphere and sensitivities of WRF, attention should also be paid to selecting the most appropriate initial and/or boundary conditions and combination of physical parametrizations. Doing so will yield more accurate model results for various application purposes or regions of interest.

To evaluate the WRF performance for wind simulation and wind energy in Portugal, Carvalho et al. (2014) compared an older reanalysis (NCEP-R2) with three recently released reanalysis datasets (ERA-Interim, NASA-MERRA, and NCEP-CFSR) as well as NCEP-GFS and NCEP-FNL analysis, distributed from the NCEP (National Centers for

Environmental Prediction) (Kalnay et al., 1996). They found that among the initial and boundary conditions of the datasets tested here, ERA-Interim reanalysis which is distributed from the ECMWF (European Center for Medium-Range Weather Forecasts) (Dee et al., 2011) likely provides the most realistic initial and boundary data because it offers the best estimates of local wind regimes and potential wind energy production. They also showed that the NCEP-GFS and NCEP-FNL analyses seem to be the best alternatives to ERA-Interim, particularly in cases where reliable forcing data are needed quickly for real-time applications. And according to Carvalho et al. (Carvalho et al., 2012), error minimization in wind simulation can be achieved by testing and choosing a suitable numerical and physical configuration for the region of interest, as well as using high-resolution terrain data.

Therefore, in addition to the different effects from GPV datasets, the selections of (combinations of) physics parametrizations are also of great importance for generating results with more accuracy, though there are many possibilities provided by the WRF model. Numerous previous studies have investigated the effects of WRF physics schemes on model performance.

Most previous studies on WRF and GPV datasets focused on

* Corresponding author.

E-mail address: cc198895@hotmail.com (C. Chen).

<https://doi.org/10.1016/j.oceaneng.2020.107379>

Received 3 January 2020; Received in revised form 10 April 2020; Accepted 11 April 2020

Available online 29 April 2020

0029-8018/© 2020 The Authors.

Published by Elsevier Ltd.

This is an open access article under the CC BY-NC-ND license

(<http://creativecommons.org/licenses/by-nc-nd/4.0/>).

operational applications such as surface temperature (Mooney et al., 2011), relative humidity, reflectivity, rainfall (Evans et al., 2012; Politi et al., 2018; Zeyaeyan et al., 2017), and WRF-Chem (Aliabadi et al., 2015; Marelle et al., 2016; Roiger et al., 2016) for a certain period in a particular geographical region (mostly land areas) and validated the model results using land-based or coast-based observations. As pointed out by Gunwani (Gunwani et al., 2017), the performance evaluation using the WRF model may agree better in terms of temperature and relative humidity compared to wind speed for different climatic zones over India. However, only a few of those previous studies attempted to apply WRF in the generation of high-resolution wind fields for ship weather routing, even though an accurate forecast of wind velocity on the ocean surface is of great importance for the safety, economic, and environmental aspects of ship weather routing.

Originally proposed by James (1957), optimum ship routing has been increasingly recognized as vital to making shipping safer, more economical, and environmentally friendly. To construct a numerical ship navigation system, Chen et al. (2013, 2015) simulated the weather and ocean in the Osaka Bay of Japan and the East China Sea using WRF with NCEP-FNL input for wind generation. Validations with JMA observations showed that high-resolution WRF calculations provided wind distributions to enable ship navigation with acceptable accuracy. The previous studies only confirmed wind simulations using land-based observations, neglecting the wind validation on the ocean surface, where ships stay. Most of the other related studies also focused on the North Pacific Ocean (Hagiwara and Spaans, 1987; Takashima et al., 2009; Lin et al., 2013); the Mediterranean Sea (Delitala et al., 2010); the North Indian Ocean (Sen and Padhy, 2015); and the North Atlantic Ocean (Chen, 1978; Hinnenthal and Clauss, 2010; Shao et al., 2012).

With increasing imports of resources and renewables each year from countries in the Southern Hemisphere, including Brazil, Africa, Australia, and Asian countries like China and Japan, the number of ships on the South-North route, including bulk carriers, tankers, and liquefied natural gas (LNG) carriers, is likely to increase. Therefore, the construction of an optimum ship routing system covering the Southern Hemisphere is of great importance. However, according to Vettor and Guedes Soares (Vettor and Guedes Soares, 2016), the number of observations is still insufficient for constructing ship routing systems from wind and wave analyses in the Southern Hemisphere.

As ocean-state observation methods such as remote sensing by satellite and buoy data are limited in spatial/temporal resolution and location, high-resolution numerical weather and ocean simulations as well as validation with on-board observations could emerge as an efficient route way generating relatively accurate ocean surface wind and sea states, especially for rough-sea navigation.

A six-year on-board observation study of weather, ocean, and ship motion was conducted from 2010 using a 20,000 DWT class bulk carrier covering both the Southern and the Northern Hemispheres. Sasa et al. (2015) have studied two rough-sea navigation cases showing the reliability of our observation system by validating ocean waves with simulations. As a next-step study, Lu et al. (2017) focused on three rough-sea navigations in the Southern Hemisphere, in an attempt to clarify proper weather and ocean generation methods for ship routing. However, the limited number and areas of rough seas studied lower the strength of the evidence.

In this study, to further investigate the uncertainty of GPV datasets and WRF modeling approaches for ocean surface high-wind generation as well as develop an optimal ship routing with encountered weather data for merchant vessels, hind-cast simulations of the high-resolution WRF model were conducted for eight rough-sea cases using both the ERA-Interim, and NCEP-FNL for WRF input, covering a larger area (including both the Southern and the Northern Hemispheres) with more sufficient temporal and spatial variability (including all seasons as well as modeling approaches such as WRF-FDDA). Additionally, two groups of physics combinations were set according to Evans et al. (2012) to clarify the performances of the WRF parameterizations in terms of wind

generation across both the Southern and Northern Hemispheres. Results of WRF simulations were evaluated with on-board observations, and suggestions for ship weather routing are provided.

The paper is organized as follows. In section 2, the on-board observation system and data collection details are provided. The model configuration is provided in section 3. Validations of model results with on-board observations are shown in section 4. Finally, in section 5, conclusions of this study and suggestions for future research are summarized.

2. On-board observations and case studies

2.1. Observation vessel

A 28,000 DWT class bulk carrier transporting cargo as a tramp was used for on-board observations. The onboard measurement has been conducted since June 2010 for 6 years. However, there were mechanical failures around PCs from 2011 to 2012, and power supplies from 2014 to 2015. Measured data does not exist in most of these periods. And there were few rough sea conditions between 2015 and 2016. Thus, extracted rough sea voyages are analyzed in 2010, 2011, 2013, 2016. The carrier's routes mainly cover oceans between Asian countries and areas of the Southern Hemisphere such as the Oceania and South America, where ocean states are generally rougher than in the Northern Hemisphere due to smaller landmasses.

2.2. Observation cases

To ensure that the research conclusion is more convincing as well as enhance our understanding of rough-sea navigation, we selected eight observation cases from all experimental periods for analysis, across both the Northern (cases 1 and 2) and Southern Hemispheres (cases 3–8) and a fully seasonal variability: Spring (cases 3 and 4), Summer (case 2), Autumn (cases 1, 5, and 6), and Winter (cases 7 and 8). The blue stars in Fig. 1 show all geographical locations where the ship experienced high wind and the WRF model domains considered for these eight cases. Detailed weather and ship conditions for each observation case are shown in Table 1. Weather data including wind speed and wind direction on the ocean surface are created using the averaged values for a 10 min time series obtained every second.

The measurement system consists of the inertial measurement unit, NAV440, and other sensors which are originally installed for the ship. There are two data sources there, one is from the NAV440, another is from the VDR (Voyage Data Recorder) and Engine Data Logger connected with all the sensors inside the ship. These data are recorded into two laptops through LAN cables. The reliability of NAV440 and other sensors is already shown for real ships (Sasa et al., 2015; Sasa et al., 2019), and all the measured data can be reliable. The wind anemometer is installed on the top of the ship structure and used in daily operation of the bulk carrier, which can observe the relative wind speed and direction with little influence of air flow induced by ship structure. As measurement facilities are a height of about 30 m over sea surface, the Smith's method (Smith, 1981) was used to interpolate the measured wind to the 10-m wind velocity. Then, ship speed and course data obtained by the VDR were used to calculate the real wind velocity over ground.

3. Model configuration

3.1. Model boundary conditions

To generate ocean surface wind fields for all eight rough sea cases, version 3.8.1 of the Advanced Research WRF (ARW) is utilized in this study; it has been developed by the National Center for Atmospheric Research (NCAR) (Skamarock, W. C., 2008). The alternating PBL schemes, surface layers, cumulus schemes, radiation schemes and microphysics schemes in the ensemble are described in section 3.2. All

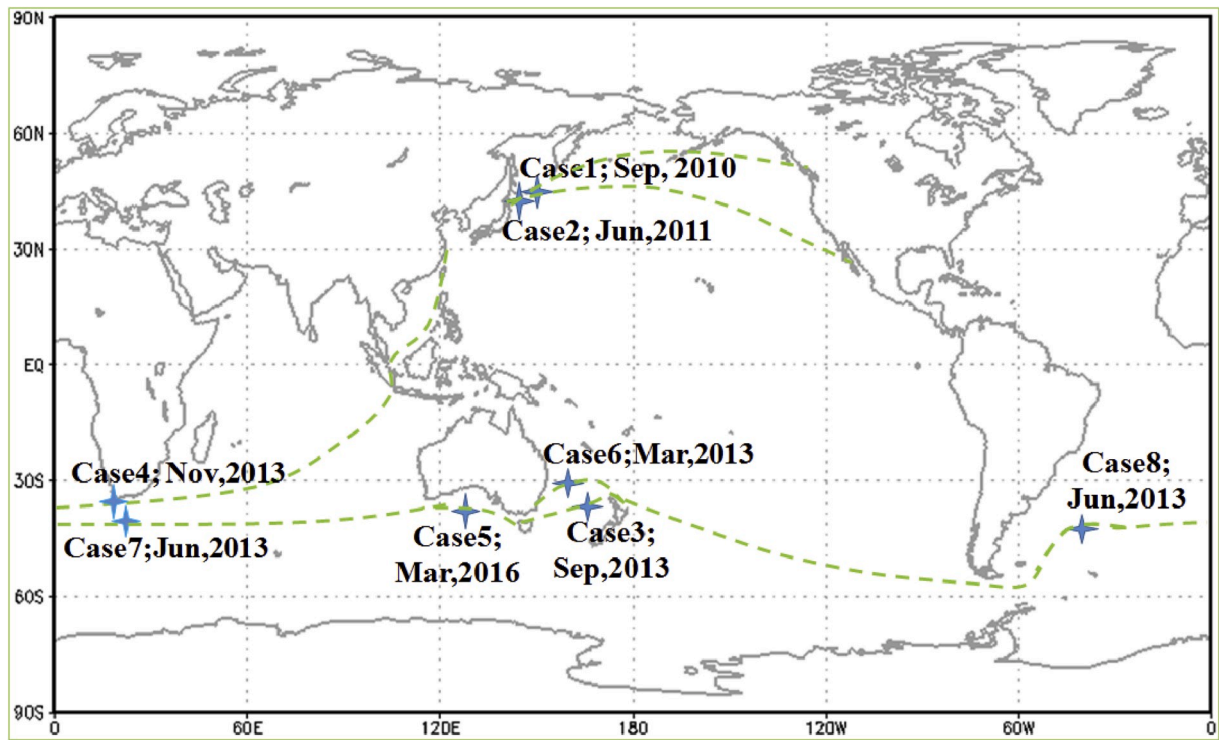


Fig. 1. Geographical locations and time of maximum pitch motions for all eight cases.

Table 1

Characteristics of weather and ship conditions in each observation case.

Case No.	Time	Model domain	Location	Maximum wind speed (m/s)	Maximum pitch amplitude (°)	Maximum wave height (m)
Case 1	Sep 2010	140–176E; 30–53N	East of Hokkaido	18.6	2.8	4.5
Case 2	Jun 2011	140–176E; 30–53N	South of Hokkaido	11.9	4.4	3.2
Case 3	Sep 2013	150–180E; 30–50S	Tasman Sea	15.9	5.7	5.1
Case 4	Nov 2013	5–38E; 25–45S	South of Africa	14.6	5.1	3.9
Case 5	Mar 2016	110–150E; 30–50S	South of Australia	14.3	4.9	4.2
Case 6	Mar 2013	135–180E; 30–50S	Tasman Sea	11.5	5.3	4.6
Case 7	Jun 2013	5–40E; 30–50S	South-East of Africa	22.3	5.2	6.5
Case 8	Jun 2013	305–335E; 30–50S	South-East of America	15.0	5.5	4.5

experiments use the Noah land surface model (Chen and Dudhia, 2001).

GPV datasets, including both the National Centers for the Environmental Prediction Final (NCEP-FNL) Operation Model Global Tropospheric Analyses (NCEP/NWS/NOAA/U.S. Department of Commerce, 2000) and the European Center for Medium-range Weather Forecasts Interim Reanalysis (ERA-Interim) (Dee et al., 2011) have been utilized as the initial and boundary conditions for WRF model. NCEP-FNL analyses offer $1^\circ \times 1^\circ$ grids covering the global region while ERA-Interim offers a spatial resolution of approximately 80 km (0.75°). Both these boundary conditions are updated every 6 h.

For all these eight cases, the WRF model was run with a horizontal resolution of 0.1° and an output time interval of 3 h. The vertical resolution of the model was 30 eta levels spaced closely together in the PBL. For each case, we chose a day window around one week that centered on the peak of the low pressures for model evaluations, in accordance with the on-board observations.

3.2. Modeling approaches and experimental design

At first, according to (Lo et al., 2008), the traditional continuous integration approach (used by Lu, 2017) could poorly simulate the forcing variables such as pressure, temperature, wind, and moisture due to the model drifting from the forcing reanalysis during long integrations. He also noted that downscaling simulations using three-dimensional (3-D) analysis nudging could constrain the error growth in large-scale circulation during the long simulation, generating realistic regional-scale patterns that are not resolved by the coarse-resolution FNL used to nudge the model. This holds especially true for meteorological fields near the surface.

In the present WRF calculations, to further understand the uncertainties of the WRF results as illustrated by Lu (2017), the grid nudging method (Stauffer and Seaman, 1990; referred to as FDDA: Four Dimensional Data Assimilation) was used to measure winds (U and V) and temperature for all vertical layers but the PBL with a time interval

between analysis times of 360 min, a ramping time period of 60 min, and nudging coefficient of 0.0003. The grid nudging method is a specific 3-D analysis whereby the atmospheric model is nudged toward time and space-interpolated analyses using a point-by-point relaxation term.

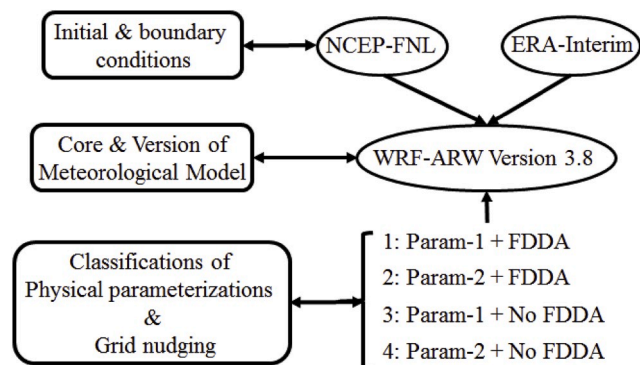
Secondly, according to Carvalho (Carvalho et al., 2012), the WRF model can be significantly affected by the choice of boundary layer parameterizations for near-surface wind simulations. It offers different options for the representations of microphysics, radiative processes, convective processes, turbulent transports as well as evolution of surface temperature and soil moisture. This study examines the performance of two combinations of physical parameterizations for real data applications in the WRF Model with regards to all eight cases, considering both the model accuracy and computational efficiency. These include cloud microphysics (WRF single moment 3 class and Eta (Ferrier) scheme) following Hong (Hong et al., 2006) and Ferrier (Ferrier et al., 2002); the cumulus parameterization (Kain-Fritsch and Bets-Miller-Janjic) following Kain and Fritsch (Kain and Fritsch, 1990) and Betts and Miller (Betts and Miller, 1986; Janjic, 1994); the PBL schemes (Yonsei-University and the Mellor-Yamada-Janjic) following Hong (Hong and Pan, 1996) and Janjic (Janjic (2002); the surface-layer physics using revised the MM5 Scheme and Eta Similarity Scheme following Jimenez (Jimenez, Pedro A., 2012) and Janjic (Janjic, Z. I., 1996, 2002); and the short and long-wave radiation schemes (Rapid Radiative Transfer Model and RRTMG scheme) following Mlawer et al. (Mlawer et al., 1997) and Iacono (Iacono et al., 2008), respectively.

In the present study, for calculating various WRF physics schemes, such as cloud microphysics, cumulus physics, shortwave/longwave radiation, PBL, and surface-layer physics, a combination of WSM 3 class, KF, Dudhia/RRTM, YSU, and Monin-Obukhov has been utilized for Param-1, while another combination of Eta (Ferrier), BMJ, RRTMG/RRTMG, MYJ, and Janjic Eta has been utilized for Param-2.

Using a single nest approach, a total of 64 WRF simulations (WRF-ARW version 3.8) were conducted for all eight cases to determine the influence of the utilization of FDDA and different physics combinations on model results, with particular emphasis on the ocean surface wind distributions. Flowchart of the model simulation and mModel settings of WRF for wind generations in these 64 numerical experiments are shown in Fig. 2.

4. Model results

As mentioned in the end of section 1, the observed wind speed following the moving vessel for all cases was averaged for a 1 h time series obtained every second for validation with WRF results (Fig. 3).



Param-1: WSM 3 Class; KF; Dudhia/RRTM; YSU; MM5-similarity

Param-2: Eta (Ferrier); BMJ; RRTMG/RRTMG; MYJ; Eta-similarity

FDDA: Four Dimensional Data Assimilation

Fig. 2. Flowchart of the model simulation and model settings of WRF for wind generations.

More detailed results analysis as well as discussions are provided in section 5.

5. Model evaluation

5.1. Evaluation statistics

To further determine the uncertainties of different GPV datasets and modeling approaches in wind simulation, the bias and root-mean-squared-error (RMSE) of the wind speed and pitch motions over observations were calculated according to Eq. (1) and Eq. (2):

$$Bias = \frac{\sum (C_i - O_i)}{N} \quad (1)$$

$$RMSE = \sqrt{\frac{\sum (C_i - O_i)^2}{N}} \quad (2)$$

where C and O represent the model calculations and on-board observations of a certain time period N for all rough-sea navigation cases, respectively. Bias indicates systematic errors, while the RMSE provides the total errors.

5.2. Divisions of model results for validations (wind strength; wind duration; wind location)

According to the final objective of the present study being selecting the best GPV dataset and WRF modeling approach for ship routing, we divide the final objective into three ones as selection of the better GPV dataset (NCEP-FNL/ERA-Interim), better nudging method (FDDA/No FDDA) as well as better physics parametrizations (Param-1/Param-2), as shown in Table 2. Table 3 shows the three group division categories, established after dividing by all cases.

The study defines clearly the differences between parameterizations (param-1/param-2), WRF modeling approaches (w/o FDDA), and GPV datasets (NCEP-FNL/ERA-Interim) for wind reanalysis over the ocean surface. At first, depending on the maximum wind speed (wind strength), all eight simulated cases are divided into four ranges as (a): $V_{max} \leq 12 \text{ m/s}$ (cases 2 and 6), (b): $12 < V_{max} \leq 15 \text{ m/s}$ (cases 4, 5, and 8), (c): $15 < V_{max} \leq 20 \text{ m/s}$ (cases 1 and 3), (d): $V_{max} > 20 \text{ m/s}$ (case 7). Secondly, considering the risk of period the ship has taken, two ranges of simulation periods (wind duration) were considered: (a) Total period (including the time period for the wind simulations for approximately one week), (b) Peak period (only for the time period corresponding to the highest wind speed for approximately one day, including both 12 h before and after the highest wind). Finally, in addition to the above two factors (wind strength and duration) affecting the generation and propagation of ocean surface waves, the performances of different GPV datasets and modeling approaches among all eight cases were compared for different locations (wind location), divided along the Northern and Southern Hemispheres.

5.2.1. Wind strength

Referring to the Beaufort scale and considering the on-board observations, four ranges of wind strength were established, as shown in Table 2, to determine the effects of various modeling approaches using different GPV datasets on wind simulation. The RMSE and bias of the simulated and on-board observed wind speeds and wind directions of these four ranges were calculated and then compared depending on 8 WRF modeling approaches. For example, consider Param-1, Param-2, FDDA, NO FDDA, FNL, and ERA in Fig. 4-A. Here, “Param-1” and “Param-2” signify the No.1 and No.2 groups of physics options for the cloud microphysics scheme, cumulus scheme, long wave and short wave radiation schemes, and PBL scheme shown in Fig. 2, respectively; FDDA and NO FDDA signify the utilization and non-utilization of the grid nudging method, respectively; and FNL and ERA signify the utilization

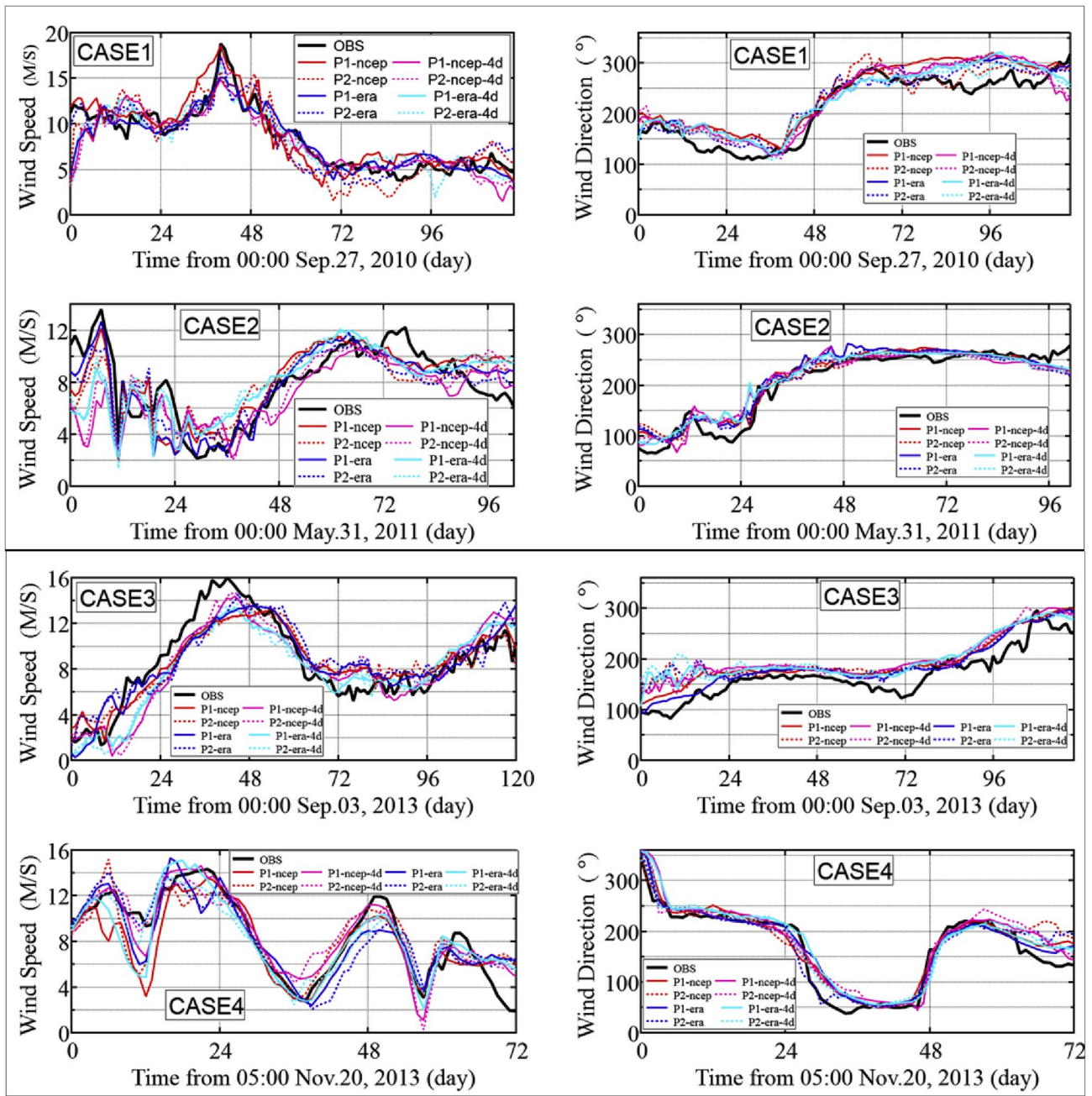


Fig. 3. Comparisons of WRF simulated wind speed and direction and on-board observations for eight rough-sea cases. Black lines represent on-board observations, and others represent wind results using different WRF modeling approaches or GPV datasets.

of the GPV datasets of NCEP-FNL and ERA-Interim, respectively.

Fig. 4 shows the RMSE and Bias values of wind speed by wind strength. Fig. 4-A and Fig. 4-C show all RMSE and Bias values for these four ranges of wind strength by all kinds of WRF simulations, Fig. 4-B and Fig. 4-D show the averaged RMSE and Bias values of wind speed for them, respectively.

At first, it can be clearly seen in Fig. 4-A and Fig. 4-B that compared with weak and strong winds such as $V_{max} < 12\text{m/s}$ and $V_{max} > 20\text{m/s}$, all WRF simulations tend to perform better for intermediate wind conditions including $12\text{m/s} \leq V_{max} \leq 15\text{m/s}$ and $15\text{m/s} < V_{max} \leq 20\text{m/s}$. This result coincides with conclusions made by D.Carvalho (2014). Then, in Fig. 4-C and Fig. 4-D, WRF simulations tend to underestimate more of the extremely high wind, such as for case 7 where $V_{max} > 20\text{m/s}$.

A better performance by “Param-2” for generating weak wind can be found in Fig. 4-C (a relatively large difference in absolute bias), i.e., $V_{max} < 12\text{m/s}$ and $12\text{m/s} \leq V_{max} \leq 15\text{m/s}$ while “Param-1” has an opposite tendency to generate better results for high wind, i.e., $15\text{m/s} \leq V_{max} \leq 20\text{m/s}$ and $V_{max} > 20\text{m/s}$.

Besides, the NO-FDDA modeling approach seems to perform better than FDDA. The reason could be that the grid nudging method used here tends to underestimate wind strength because of its smoothing effects, as shown in Fig. 4-A and Fig. 4-C, which was also pointed out by Vincent C L (Vincent and Hahmann, 2015) and Nakano (2010).

Regardless of the GPV datasets, the ERA-Interim dataset has relatively smaller RMSE values compared to NCEP-FNL, but it should be noticed here that ERA-Interim tends to underestimate more of relatively higher wind conditions as shown in Fig. 4-C ($12\text{m/s} \leq V_{max} \leq 15\text{m/s}$,

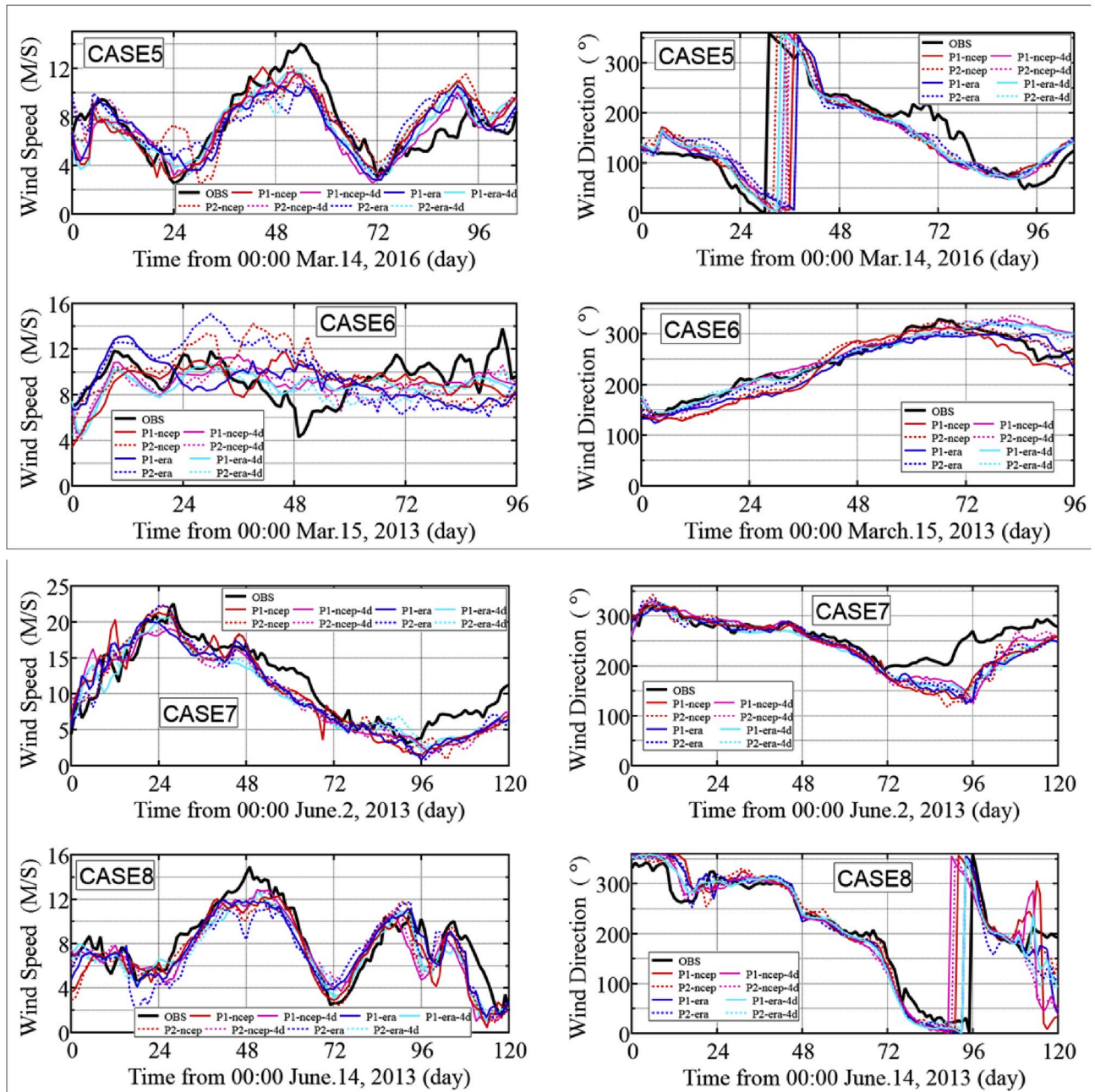


Fig. 3. (continued).

Table 2

Objectives of WRF simulations.

Experimental objectives
1 Comparisons of GPV dataset performance for ship weather routing
2 Comparisons of WRF performance with and without FDDA (analysis nudging) for ship weather routing
3 Comparisons of WRF performance with two different combinations of physics parametrizations for ship weather routing

15 m/s < V_{max} ≤ 20 m/s, V_{max} > 20 m/s).

Fig. 5 shows the RMSE and Bias values of wind direction by wind strength. Fig. 5-A and Fig. 5-B show that RMSE for intermediate wind speeds is between those for lower and higher wind speeds, respectively.

Then, Fig. 5-C shows that the WRF tends to generate relatively clockwise wind for most cases, except for the highest wind in case 7,

Table 3

Standard and details of group divisions for the bias and RMSE of wind simulations.

Group divisions	Details of group divisions			
Wind Strength	$V_{max} < 12$ m/s	$12 \text{ m/s} \leq V_{max} \leq 15 \text{ m/s}$	$15 \text{ m/s} < V_{max} \leq 20 \text{ m/s}$	$V_{max} > 20$ m/s
Wind Duration	Total period (approximately one week)		Peak period (approximately one day)	
Wind Location	Northern Hemisphere		Southern Hemisphere	

where WRF did not accurately simulate the wind direction for a long time period (approximately two days of weak wind; wind speed less than 5 m/s) compared with on-board observations. This may be due to the

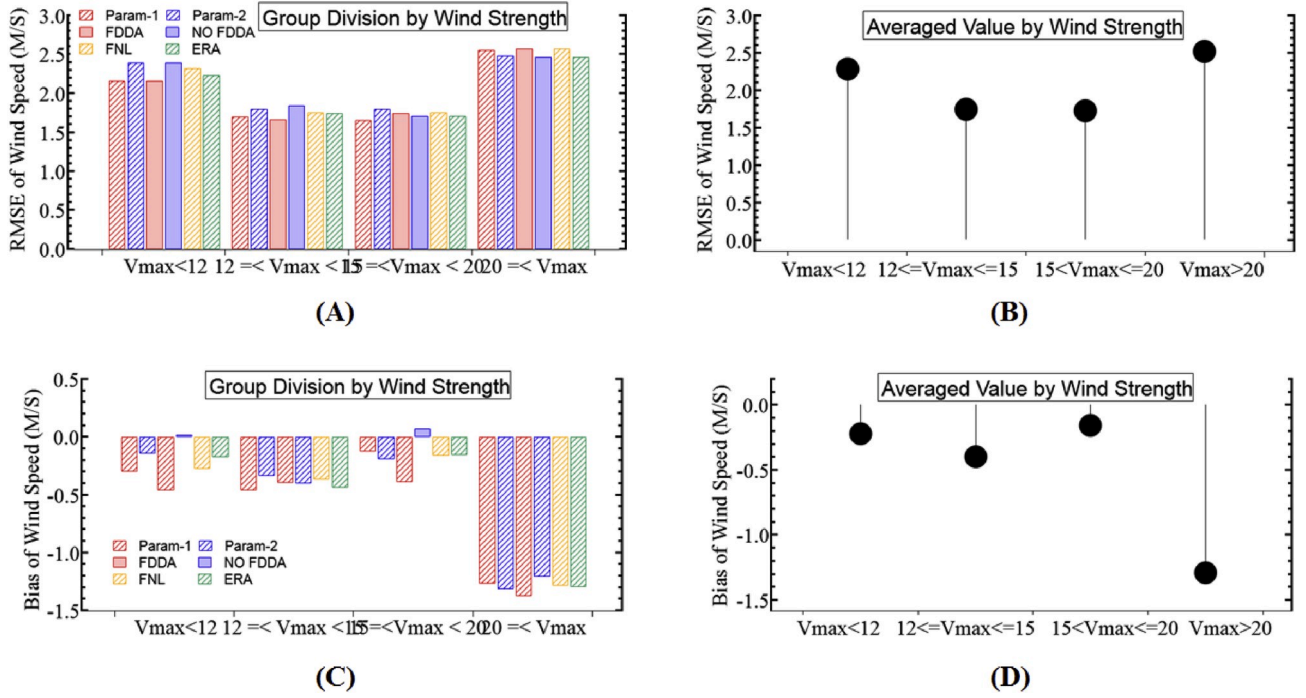


Fig. 4. RMSE and Bias values of wind speed by wind strength, where “Param-1” and “Param-2” signify the No.1 and No.2 group of physics options for the cloud microphysics scheme, cumulus scheme, long wave and short wave radiation schemes, and planetary boundary layer scheme shown in Table 2, respectively; FDDA and NO FDDA signify the utilization and non-utilization of the grid nudging method, respectively; and FNL and ERA signify the utilization of the GPV datasets of NCEP-FNL and ERA-Interim, respectively.

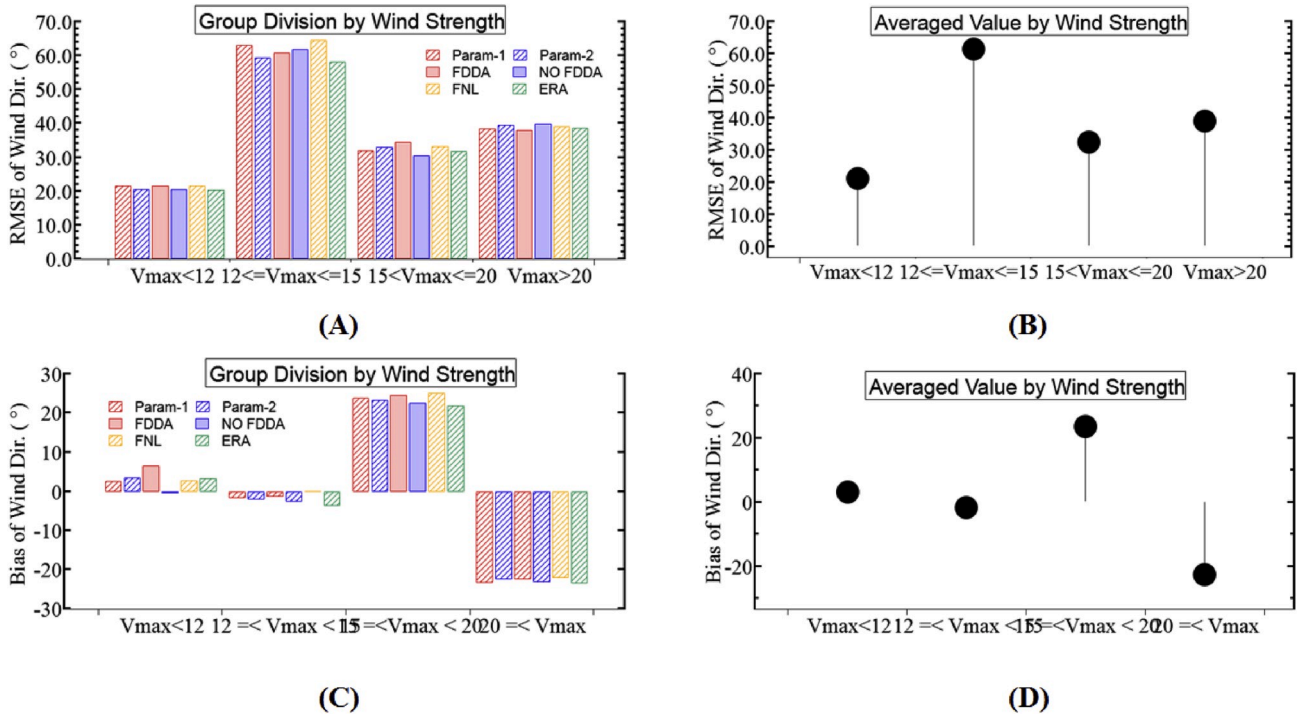


Fig. 5. RMSE and Bias values of wind direction by wind strength.

WRF generating wind direction with a relatively low accuracy when the wind speed is low. The “Param-2” tends to generate better wind direction for low wind while the “Param-1” performs better for high wind with smaller RMSE values in Fig. 5-A.

Generally, the ERA-Interim performs better for wind direction (shown in Fig. 5-A) while the NCEP-FNL has a smaller underestimation

in the highest wind case (shown in Fig. 5-C).

5.2.2. Wind duration

To determine the different performances of the various WRF simulations on wind generation for ship routing, especially in dangerous situations with rough seas and strong ocean surface wind, two groups,

termed “Total period” and “Peak period” were compared for all eight rough-sea cases, where the former refers to the entire period of WRF simulation for each case and the latter refers to the period around the maximum wind speed, with time lengths of approximately one week and one day, respectively. The RMSE and bias of the simulated and on-board observed wind speed and wind direction of these two groups were calculated and then compared, for all utilized WRF modeling approaches, as illustrated in section 5.2.1.

Fig. 6 shows the RMSE and Bias values of wind speed by wind duration. Fig. 6-A and Fig. 6-C show all RMSE and Bias values for the two groups (total period and peak period) of wind duration using all WRF simulations, while Fig. 6-B and Fig. 6-D show the averaged RMSE and Bias values of wind speed for these two groups.

It is clear in Fig. 6-A and Fig. 6-B that compared with “Total period” group, the “Peak period” group has smaller RMSE and absolute Bias values, which implies that the WRF tends to perform better for relatively high wind (peak period, which only includes the high wind period) as opposed to weak wind (total period, which includes both high and weak wind).

For the GPV dataset, Fig. 6-A shows a better performance of ERA-Interim than NCEP-FNL for the total period (including both weak wind and high wind periods), but an opposite tendency for the peak period (only for high wind). This shows that NCEP-FNL tends to perform better for high wind while ERA-Interim provides a better result for relatively weaker wind.

It can also be found from Fig. 6-C that the utilization of FDDA tends to increase the underestimation of wind speed owing to its smoothing effects. Regarding to the physical parameterizations, the “Param-1” performs better than “Param-2”, especially for the “Peak period” as shown in Fig. 6-C, which also agrees with the finding in Fig. 4 that “Param-1” performs better than “Param-2” in case of generation high wind speed. The reason why absolute averaged value of bias for the “Total period” is lower than that of the “Peak period” is the underestimation of extremely high wind for the peak period, as shown for cases 3, 5, and 8 in Fig. 3.

Fig. 7 shows the RMSE and Bias values of wind direction by wind duration. All panels in Fig. 7 show that WRF can generate better wind

direction for high wind (peak period) than for weak wind (total period), agreeing with D. Carvalho (2014). Fig. 7-A shows that “Param-1” provides a more accurate result than “Param-2” for peak wind. This also agrees with the above analysis from RMSE values of wind speed by wind strength in Fig. 4. FDDA, when utilized with a smoothing effect, tends to improve the performance of wind direction generation with a greater effect on high wind than weak wind (Fig. 7-A). For the GPV dataset, all three figures in Fig. 7 show that ERA-Interim performs better than NCEP-FNL for the generation of wind direction.

Then, in Fig. 7-C, the positive bias values indicate that WRF tends to generate relatively clockwise wind for most cases. Fig. 7-C also shows a relatively larger negative effect of FDDA on generating the wind direction for weak wind (“Total period”) than high wind (“Peak period”).

5.2.3. Wind location

Finally, the present study tries to focus on the different effects of the 8 above-mentioned WRF modeling approaches on the generation of ocean surface wind for the Southern and Northern Hemispheres.

Fig. 8 shows the RMSE and Bias values of wind speed by wind duration. Fig. 8-A and Fig. 8-C show all RMSE and Bias values for the two groups (Northern Hemisphere and Southern Hemisphere) of wind location using all WRF simulations. Fig. 8-B and Fig. 8-D show the averaged RMSE and Bias values of wind speed for these two groups using all WRF modeling approaches.

All these four panels in Fig. 8 clearly show that compared with the “Southern Hemisphere” group, the “Northern Hemisphere” group has relatively smaller RMSE and absolute Bias values, which implies that these WRF modeling approaches tend to perform better for the Northern Hemisphere. Fig. 8-A further shows that “Param-1” provides a better result than “Param-2”, owing to its better performance for high wind, which also agrees with the above analysis for the RMSE values of wind speed by wind strength. Fig. 8-C again shows that FDDA with a smoothing effect tends to underestimate wind more significantly, agreeing with the results obtained for bias values of wind speed by wind strength in Fig. 4-C. Regarding to GPV datasets, ERA-Interim performs slightly worse than NCEP-FNL in “Southern Hemisphere”, possibly due to its poorer performance in generating high wind such Case 7 (the

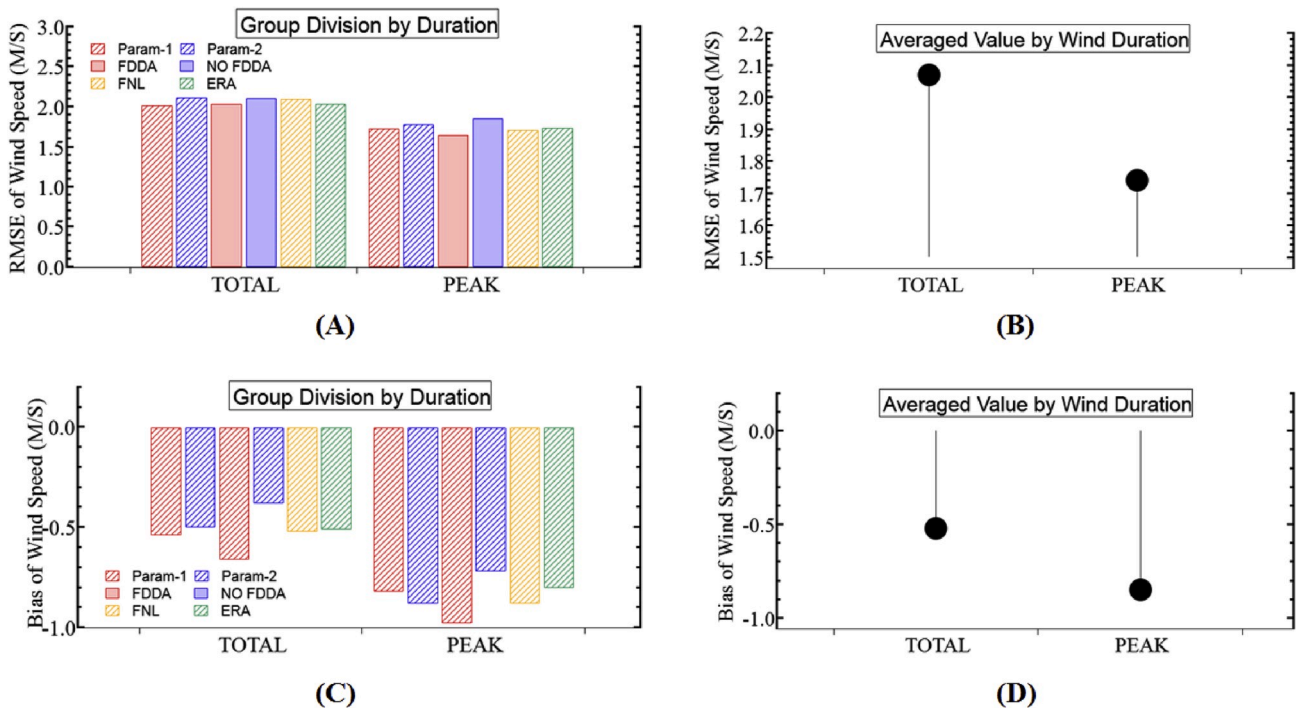


Fig. 6. RMSE and Bias values of wind speed by wind duration.

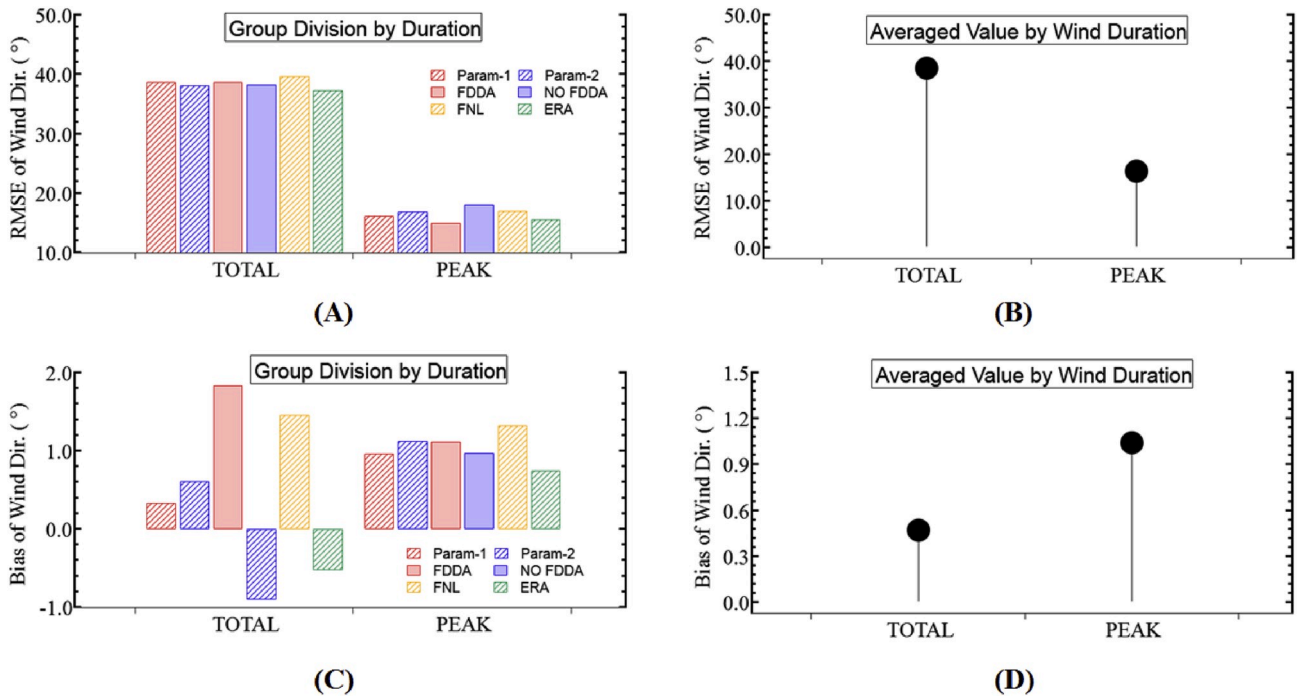


Fig. 7. RMSE and Bias values of wind direction by wind duration.

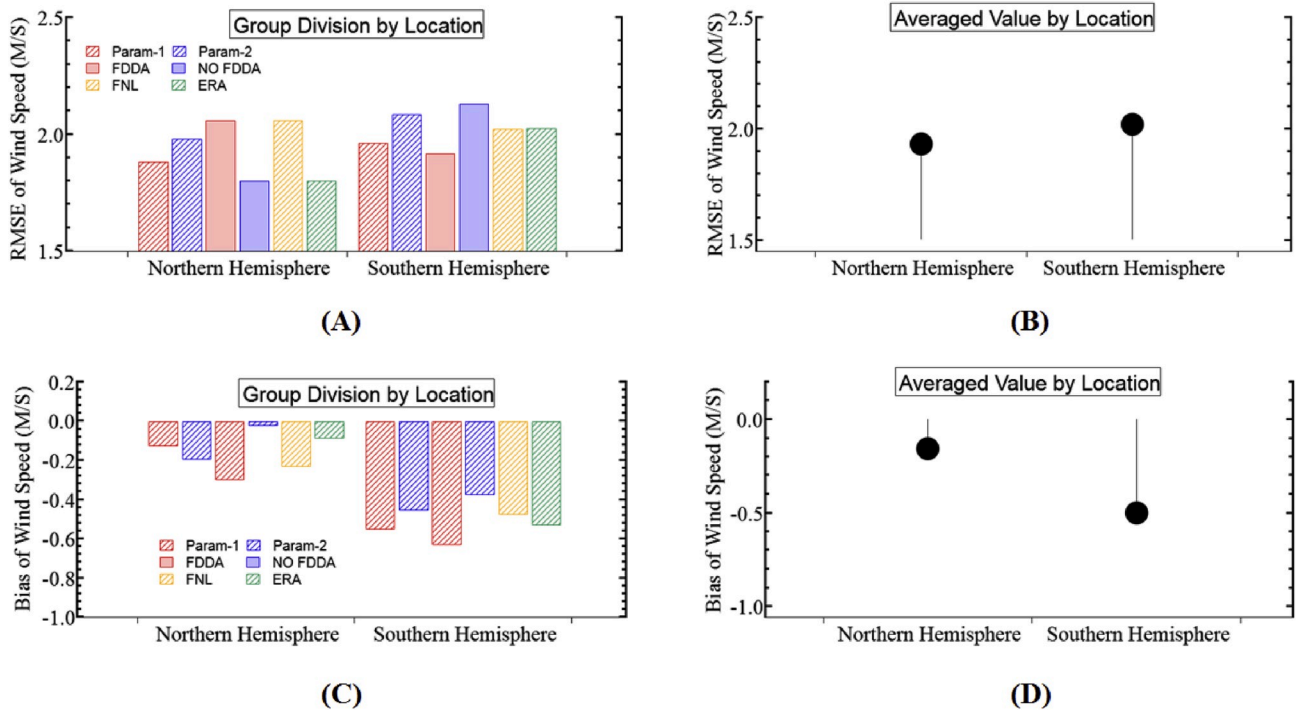


Fig. 8. RMSE and Bias values of wind speed by wind location.

highest wind, as shown in Fig. 3).

Fig. 9 shows the RMSE and Bias values of wind direction by wind location. Fig. 9-A and Fig. 9-B show that WRF has a tendency to generate better wind direction for the “Northern Hemisphere” group than the “Southern Hemisphere”. Also, Fig. 9-C shows that “Param-2” provides better results than Param-1, owing to the poorer performance of “Param-1” for the “Northern Hemisphere” group. Moreover, the use of FDDA with a smoothing effect tends to further delay the accurate estimation of wind direction, especially for extreme high wind periods, as shown in

Fig. 4. Furthermore, for the GPV dataset, all figures indicate a better performance of ERA-Interim than NCEP-FNL for the generation of wind direction.

Then, in Fig. 9-C, the positive bias values indicate that WRF tends to generate relatively clockwise wind for most cases. Although it appears that the bias values of the “Northern Hemisphere” group are higher than those of the “Southern Hemisphere” group from Fig. 9-C, it should be noted that the bias values are a combination of several cases that also include the high negative values of the latter group, leading to lower bias

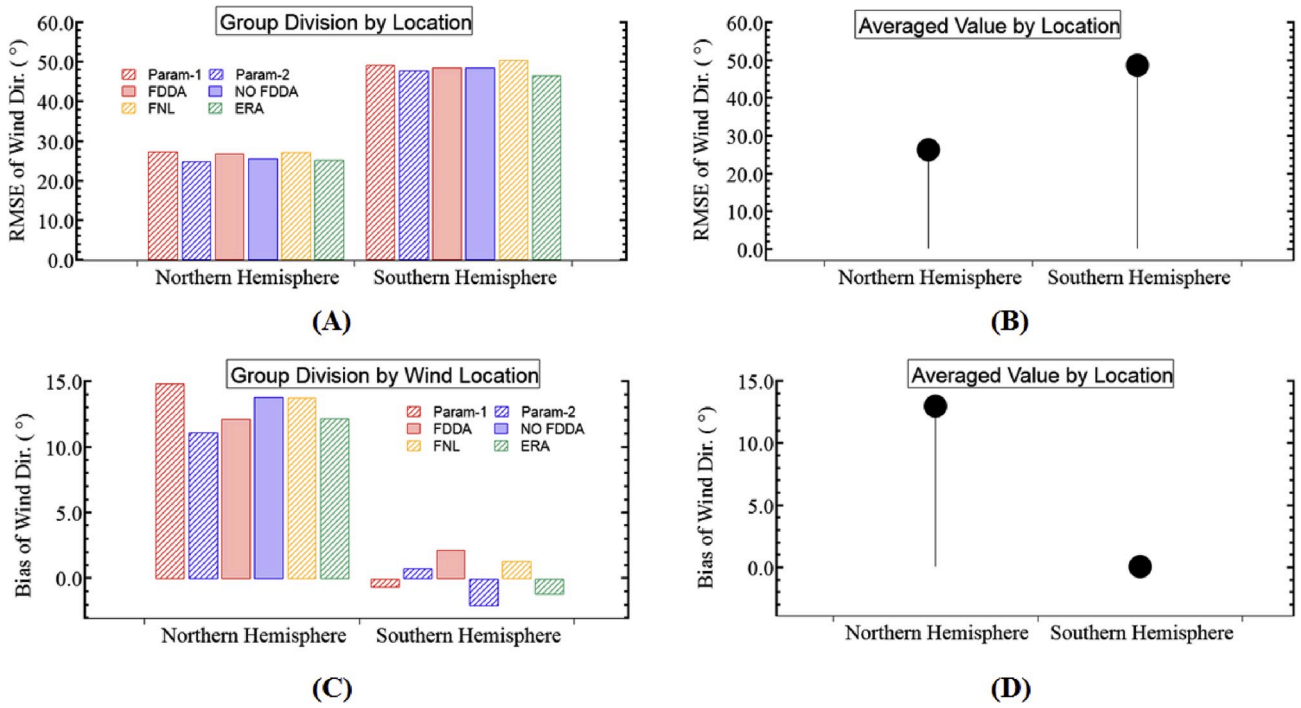


Fig. 9. RMSE and Bias values of wind direction by wind location.

values for the latter group as shown in Fig. 9-C.

5.2.4. Evaluation WRF performance for all cases

To have an overall division of WRF performance for all cases, Fig. 10 is given, where Fig. 10-A and Fig. 10-B are the averaged RMSE and Bias values of wind speed of all WRF simulations in all eight cases while Fig. 10-C and Fig. 10-D are those values of wind direction.

In terms of the physical parametrizations, the smaller RMSE value in Fig. 10-A and a larger one in Fig. 10-C show that the “Param-1” performs better for wind speed, same as other studies (XM Hu et al., 2010) and

(MEB Frediani et al., 2016), but worse for wind direction when compared with “Param-2”. The reason why the Bias value of “Param-1” is smaller than “Param-2” is that the “Param-1” performs better for high wind while the “Param-2” has an opposite tendency, which can be illustrated in Fig. 4-C and Fig. 5-C.

Compared with the ERA-Interim, the NCEP-FNL tends to over-estimate more of wind speed, as shown in Fig. 10-A. And it can be shown in Fig. 10-C and Fig. 10-D that the ERA-Interim has a better performance on wind direction than the NCEP-FNL, which agrees with another study by (Carvalho D, 2014) that WRF simulation driven with ERA-Interim

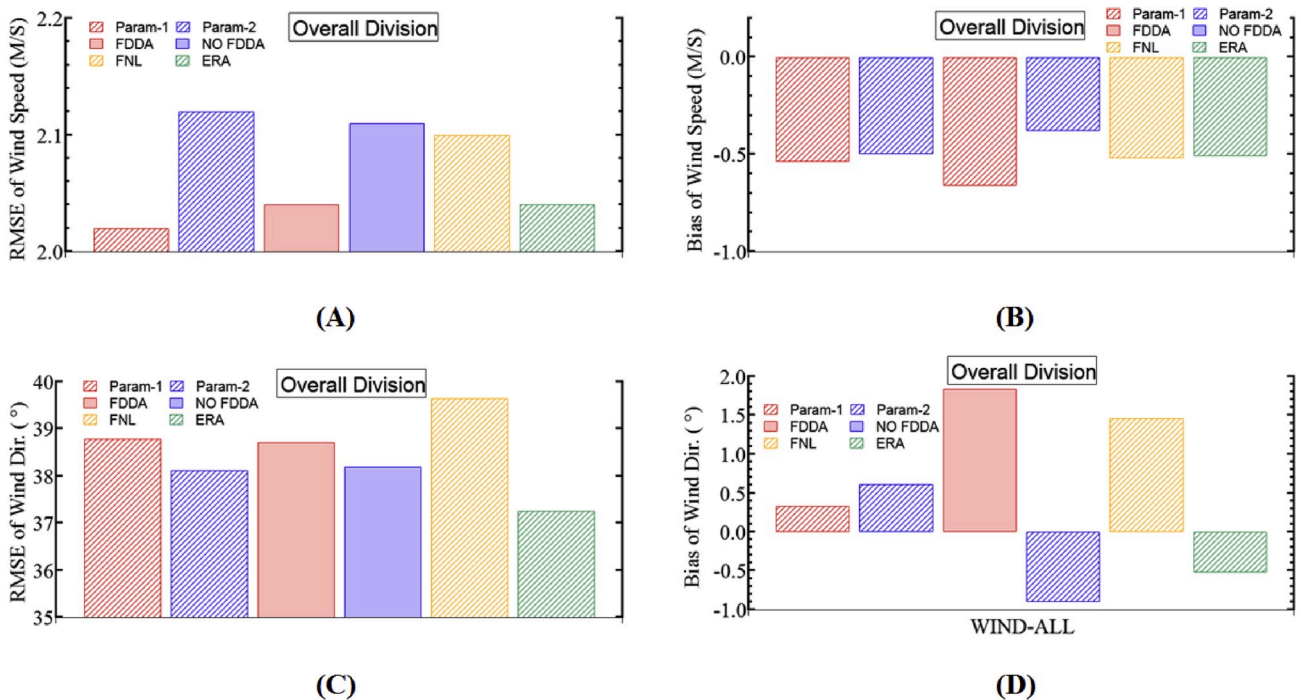


Fig. 10. An overall division of WRF performance for all cases.

presents the lowest errors for the wind direction.

Owing to its smoothing effects, as pointed out by Vincent C L (Vincent and Hahmann, 2015) and Nakano (2010), the utilization of FDDA can increase the underestimation of wind speed as shown in Fig. 10-B, and the smaller RMSE value of “FDDA” in Fig. 10-A results from the relatively large underestimation of low wind cases as shown in Fig. 4-A. Regarding to the wind direction, the FDDA also has a larger effect on low wind generation than high wind, as shown in Fig. 7-C and Fig. 8-C.

6. Discussions on uncertainties of WRF modeling approaches and GPV datasets

6.1. Influences of FDDA approach on model results

Generally, regional climate models (RCMs) like the WRF connect global driving fields only through the lateral boundaries. Meanwhile, if model domains of RCM are set in zones where global circulation mechanisms and upper air large-scale patterns exist, these patterns are possibly not very well reproduced by the RCM because it may develop unrealistic circulation patterns and generate inaccuracy of important large-scale features. The FDDA can help constrain the RCM by choosing 3-D variables from the GPV analysis.

As Lo et al. (2008) pointed out, compared with the traditional continuous integration approach that poorly simulates the forcing wind during long integrations as the model drifts away from the forcing reanalysis, 3-D analysis nudging can constrain the error growth in large-scale circulation during long downscale simulations. Thus, it generates realistic regional scale patterns that are not resolved by the coarse-resolution FNL that is used to nudge the model, especially for meteorological fields near the surface.

Miguez-Macho et al. (2004) also noted that dynamic downscaling models can develop unrealistic circulation patterns if only the lateral boundaries are considered for global input, whereas applying a nudging term can preserve important large-scale features within the dynamic downscaling process.

However, the analyses in section 5.2 identified a smoothing effect from the grid nudging method in the generation of wind speed by WRF simulations for extremely high wind (shown in Fig. 4-A and Fig. 5-A), leading to greater underestimation. Therefore, the utilization of the grid nudging method should not be recommended for generating ocean surface winds to be used in ship weather routing, especially in rough-sea navigation.

6.2. Sensitivity to physical parametrizations

According to the RMSE and bias analyses provided in section 5.2, “Param-1” seems to perform better for generating relatively higher wind than “Param-2” (Fig. 4-A and Fig. 5-A). “Param-1” generates more accurate results for higher wind ($V_{max} > 20\text{m/s}$, $15\text{m/s} < V_{max} \leq 20\text{m/s}$) while “Param-2” performs better for weaker wind ($V_{max} < 12\text{m/s}$ and $12\text{m/s} \leq V_{max} \leq 15\text{m/s}$).

To elucidate the cloud microphysics mechanism by which moisture is removed from the air, based on other thermodynamic and kinematic fields represented within the WRF model, WSM-3 class, which represents the WRF single-moment 3 class Microphysics Scheme and Eta (Ferrier) were used for “Param-1” and Param-2, respectively. Comparing some observed features (track, maximum sustained wind, and sea level pressure) with simulations in his study on the impact of microphysics schemes in the simulation of the cyclone Phailin using the WRF model, BK Mahala (Mahala et al., 2015) found that simulations with the WRF Single Moment-3 (WSM3) class microphysics scheme compare well with observations. In another study on the tropical cyclone Mora over the Bay of Bengal, Chutia (Chutia, Lakhima, et al., 2018) showed that the convergence of surface winds which pick up heat and moisture from the ocean were also well simulated using the WSM3, showing better

performance with the least RMSE compared to all other schemes, despite the fact that all schemes overestimated the observed MSW and MSLP during the storm period. In our present study, the “Param-1” group has a better performance, which also uses the WSM3 as the microphysics scheme.

With the cumulus physics scheme, the mass-flux type Kain-Fritsch (KF) and the adjustment type Bets-Miller-Janjic (BMJ) were used for “Param-1” and Param-2, respectively. Fersch (Fersch and Kunstmann, 2014) found that for hot and dry regions like the Sahara, the BMJ scheme outperformed the KF scheme for precipitation generation in their study on water budgets; however, the KF in “Param-1” may perform better than the BMJ in “Param-2” owing to the present study focusing on relatively wet regions of the ocean surface.

It is known that near-surface momentum depends on vertical diffusion schemes in the unstable regime, and the shapes of the vertical profiles are determined by PBL mixing algorithms. Here first-order closure schemes, i.e., Yonsei University scheme (YSU) and the turbulent kinetic energy (TKE) closure scheme denoted the Mellor Yamada Janjic (MYJ) scheme, were utilized for “Param-1” and Param-2, respectively. According to Hu (XM Hu et al., 2010), due predominantly to differences in the vertical mixing strength and entrainment of air from above the PBL, the WRF simulations with the YSU and ACM2 schemes provide much less bias than with the MYJ scheme. He also showed that simulations with the MYJ scheme produced the coldest and moistest biases in the PBL. Moreover, Frediani (MEB Frediani et al., 2016) pointed out that the YSU scheme accounts for counter-gradients and entrainment at the PBL top, which translates into stronger vertical mixing, while the known weak vertical mixing in the MYJ scheme is reflected in the increasing bias during PBL diurnal evolution. Agreeing with their findings, the present study finds that the combination of “Param-1” with the YSU performs better than that of “Param-2” with MYJ for simulating strong winds.

The surface layer parametrizations contribute to near-surface variability in both convective and stable regimes. Determined by the PBL schemes selected above, two kinds of surface-layer physics including MM5-similarity and Eta-similarity were used for the “Param-1” and Param-2, respectively. Based on Monin-Obukhov, Janjic Eta includes parameterizations of a viscous sub-layer and computes the surface fluxes by an iterative method. In a study comparing the performance of two surface layer parameterizations (MM5-similarity/Eta-similarity schemes) over a tropical site in southeast India, K Hari Prasad (K Hari Prasad et al., 2016) found that although both schemes depict a systematic bias in various surface layer parameters, the predicted values with the MM5-similarity scheme are in better agreement with observational estimates as indicated by the qualitative and quantitative comparisons of results. They also argued that the differences in the results of the two schemes can be attributed to the variation in the empirical stability correction functions and the stability regimes used in the two schemes. In a study of WRF surface wind, temperature and water vapour mixing ratio for the Portuguese territory, Ferreira et al. (2008) found that the variation of the SL and PBL schemes have a significant influence on the wind prediction (especially for cold seasons) and also that the SL-PBL parameterization set MM5-YSU is the one that presents better results in the wind simulation. Similarly, in the present study, the MM5-similarity scheme used for “Param-1” also contributes to the better performance of “Param-1” in simulating high wind.

6.3. Uncertainty of GPV datasets

Finally, to consider the uncertainty of the boundary conditions for the dynamical downscaling, two global atmospheric reanalysis products with different models, observations, and data assimilation for the dataset-making process were employed for the regional simulations. For instance, ERA-Interim uses four-dimensional variational analysis assimilation, while NCEP-FNL uses a 3-D variational analysis.

In almost all figures shown in section 5.2, comparisons of the RMSE

indicate that ERA-Interim performs better than NCEP-FNL for weak wind ($V_{max} < 12\text{ m/s}$ and $12\text{ m/s} \leq V_{max} \leq 15\text{ m/s}$) and long periods ("Total period"), while NCEP-FNL generates a smaller error than ERA-Interim for other situations such as high wind ($V_{max} > 20\text{ m/s}$) and a short peak period ("Peak period"). This further illustrates that ERA-Interim tends to be better for longer period wind analysis, such as studies on practical applications for offshore wind energy, while NCEP-FNL should be recommended for shorter period but higher wind analysis, thereby enabling navigational safety in ship weather routing.

7. Conclusions

In this study, the performance of the RCM WRF was studied as well as validated against on-board observations for eight rough-sea cases, considering approaches that include two different boundary conditions, two groups of physics parametrizations, and the optional grid nudging method. Eight cases with durations of few days each were selected for the study. Owing to their geographic positions, the cases represent open-ocean conditions. Through these WRF simulations of ocean surface wind and the validations against on-board observations, we can draw the following conclusions for WRF simulations in open and rough seas:

- (1) For wind strength, WRF simulations provide more accurate results for intermediate wind speeds (cases 1, 3, 4, 5, and 8; between 12 and 20 m/s) than for low and high wind speeds (cases 2 and 6; less than 12 m/s, and case 7, higher than 20 m/s). This may be due to the downscaling effects of the RCM in calculating physical phenomena. The present study also illustrates that WRF can generate a better wind direction for high winds than for low winds.
- (2) For locations, the model simulations provide more accurate results for the Northern Hemisphere than for the Southern Hemisphere, which may result from the fact that more land-based observation stations are available in the Northern Hemisphere, providing relatively sufficient data for both high spatial and temporal resolution for three (NCEP-FNL) or four-dimensional (ERA-Interim) variational assimilation analysis.
- (3) For GPV datasets, we find from the present study that although WRF simulations do not properly generate the peak wind speed (timing of maximum wind speed) compared to on-board observations, NCEP-FNL tends to simulate more accurate results for higher winds compared to ERA-Interim. ERA-Interim is suitable for longer periods, while NCEP-FNL has additional capabilities to analyze the extremes. Therefore, NCEP-FNL is recommended for ship routing because of its improved representation of strong winds during rough-sea conditions, which is of great importance for ship safety and optimal routing. Additionally, the ERA-Interim dataset performs better than NCEP-FNL at generating wind direction.
- (4) For the grid-nudging method (FDDA), the present study finds that wind strength was more greatly underestimated through simulation due to the smoothing effect in generating extremely high winds. Therefore, the grid nudging method should not be recommended to generate ocean surface wind for ship weather routing, especially in the rough seas.
- (5) Owing to the fact that regional models cannot resolve smaller spatial and temporal scales, physically based parameterization schemes have been proposed for solving these physical processes. The parameterizations used for "Param-1" seem to better estimate strong ocean surface wind for open and rough seas than those for "Param-2", although most of the parameterizations used for "Param-2" are more complex schemes. There are two main reasons why more complex schemes may not necessarily lead to consistently better results, even though they can improve physical realism and are able to simulate physical processes more realistically. One is that the more realistic physics used in more

complex schemes may expose other model deficiencies such as model resolution and initialization. Additionally, other physical parameterizations have often been developed and tuned to function with simpler schemes. Therefore, the relatively simple parameterizations used for "Param-1" are recommended for ship weather routing, especially after considering the efficiency and usage of computerization and the better performance of "Param-1" in generating high wind.

- (6) Finally, from the viewpoint of optimum ship routing, a combination of the NCEP-FNL dataset with high-resolution WRF modeling using "Param-1" and No-FDDA is recommended due to its higher accuracy when estimating relatively high wind speeds over the ocean surface; while the possible underestimation by ERA-Interim, "Param-2" and FDDA will bring the ship to a high risk and thus should be avoided. It should also be noticed here that the ERA5 data, with a higher spatial and temporal resolution than ERA-Interim data, should be used for future studies. Besides, the observed cases are still limited at present, and further analysis of newly-observed data by another vessel will be conducted in the future study.

Declaration of competing interest

The authors declare that they have no known competing financial interests or personal relationships that could have appeared to influence the work reported in this paper.

CRediT authorship contribution statement

Chen Chen: Conceptualization, Methodology, Visualization, Investigation. **Kenji Sasa:** Supervision, Validation, Writing - review & editing, Project administration, Resources. **Teruo Ohsawa:** Methodology, Supervision. **Jasna Prpić-Oršić:** Supervision.

Acknowledgements

We would like to thank Shoei Kisen Kaisha Ltd., Northstar Shipping Management Ltd., and the crew of the bulk carrier who collected the data used in this research. This study was financially supported by a Grant-in-Aid for Early-Career Scientists '19K15251' (2019–2021, represented by Chen Chen) and Fostering Joint International Research (B) '18KK0131' (2018–2022, represented by Kenji Sasa) under Grants-in-Aid for Scientific Research, Japan Society for the Promotion of Science. This study was also supported by the Croatian Science Foundation under the project IP-2018-01-3739. Appreciation is also extended to Mr. Taishi Yonemura, who contributed to this work.

References

- Míguez-Macho, G., Stenchikov, G.L., Robock, A., 2004. Spectral nudging to eliminate the effects of domain position and geometry in regional climate model simulations. *J. Geophys. Res.: Atmosphere* 109, D13.
- Aliabadi, A.A., Staebler, R.M., Sharma, S., 2015. Air quality monitoring in communities of the Canadian Arctic during the high shipping season with a focus on local and marine pollution. *Atmos. Chem. Phys.* 15 (5), 2651–2673.
- Betts, A.K., Miller, M.J., 1986. A new convective adjustment scheme. Part II: single column tests using GATE wave, BOMEX, and arctic air-mass data sets. *Q. J. R. Meteorol. Soc.* 121, 693–709.
- Carvalho, David, et al., 2012. A sensitivity study of the WRF model in wind simulation for an area of high wind energy. *Environ. Model. Software* 33, 23–34.
- Carvalho, D., Rocha, A., Gómez-Gesteira, M., et al., 2014. WRF wind simulation and wind energy production estimates forced by different reanalyses: comparison with observed data for Portugal[J]. *Appl. Energy* 117, 116–126.
- Cha, D.H., Wang, Y., 2013. A dynamical initialization scheme for real-time forecasts of tropical cyclones using the WRF model. *Mon. Weather Rev.* 141 (3), 964–986.
- Chen, Henry., 1978. *A dynamic program for minimum cost ship routing under uncertainty*. Diss. Massachusetts Institute of Technology.
- Chen, F., Dudhia, J., 2001. Coupling an advanced land surface–hydrology model with the Penn State–NCAR MM5 modeling system. Part I: Model implementation and sensitivity. *Monthly weather review* 129, 569–585.

- Chen, Chen, Shigeaki Shiotani, Kenji, Sasa, 2013. Numerical ship navigation based on weather and ocean simulation. *Ocean. Eng.* 69, 44–53.
- Chen, Chen, Shiotani Shigeaki, Sasa, Kenji, 2015. Study on a Numerical Navigation System in the East China Sea. *Appl. Ocean Res.* 53, 257–266.
- Davis, C., et al., 2008. Prediction of landfalling hurricanes with the advanced hurricane WRF model. *Mon. Weather Rev.* 136 (6), 1990–2005.
- Dee, D.P., Uppala, S.M., Simmons, A.J., et al., 2011. The ERA-Interim reanalysis: configuration and performance of the data assimilation system[J]. *Q. J. Roy. Meteorol. Soc.* 137 (656), 553–597.
- Delitala, A.M.S., et al., 2010. Weather routing in long-distance Mediterranean routes. *Theor. Appl. Climatol.* 102 (1–2), 125–137.
- Evans, J.P., Ekström, M., Ji, F., 2012. Evaluating the performance of a WRF physics ensemble over South-East Australia. *Clim. Dynam.* 39 (6), 1241–1258.
- Ferreira, A.P., Castanheira, J.M., Rocha, A., et al., 2008. Estudo de sensibilidade das previsões de superfície em Portugal pelo WRF face à variação das parametrizações físicas.
- Ferrier, B.S., Lin, Y., Black, T., Rogers, E., DiMego, G., 2002. Implementation of a new grid scale cloud and precipitation scheme in the NCEP Eta model. In: *Proceedings of the 15th Conference on Numerical Weather Prediction*. American Meteorological Society, San Antonio, Tex, USA, pp. 280–283.
- Fersch, B., Kunstmann, H., 2014. Atmospheric and terrestrial water budgets: sensitivity and performance of configurations and global driving data for long term continental scale WRF simulations. *Clim. Dynam.* 42, 9–10, 2367–2396.
- Frediani, M.E.B., et al., 2016. Evaluation of PBL parameterizations for modeling surface wind speed during storms in the northeast United States. *Weather Forecast.* 31 (5), 1511–1528.
- Gunwani, P., Mohan, M., 2017. Sensitivity of WRF model estimates to various PBL parameterizations in different climatic zones over India. *Atmos. Res.* 194, 43–65.
- Hagiwara, H., Spaans, J.A., 1987. Practical weather routing of sail-assisted motor vessels. *J. Navig.* 40 (1), 96–119.
- Hari Prasad, K.B.R.R., et al., 2016. Assessment of surface layer parameterizations in ARW using micro-meteorological observations from a tropical station. *Meteorol. Appl.* 23 (2), 191–208.
- Hinnenthal, J., Clauss, G., 2010. Robust Pareto-optimum routing of ships utilising deterministic and ensemble weather forecasts. *Ships Offshore Struct.* 5 (2), 105–114.
- Hong, S.Y., Pan, H.L., 1996. Nonlocal boundary layer vertical diffusion in a medium-range forecast model. *Mon. Weather Rev.* 124 (10), 2322–2339.
- Hong, S.Y., Noh, Y., Dudhia, J., 2006. A new vertical diffusion package with an explicit treatment of entrainment processes. *Mon. Weather Rev.* 134 (9), 2318–2341.
- Hu, X.M., Nielsen-Gammon, J.W., Zhang, F., 2010. Evaluation of three planetary boundary layer schemes in the WRF model. *J. Appl. Meteorol. Climatol.* 49 (9), 1831–1844.
- Iacono, M.J., Delamere, J.S., Mlawer, E.J., Shephard, M.W., Clough, S.A., Collins, W.D., 2008. Radiative forcing by long-lived greenhouse gases: calculations with the AER radiative transfer models. *J. Geophys. Res.* 113, D13103.
- James, Richard W., 1957. Application of wave forecasts to marine navigation.
- Janjic, Z. I. “The Surface Layer in the NCEP Eta Model. Eleventh Conference on Numerical Weather prediction.” Norfolk, VA, 19–23 August 1996. American Meteorological Society, Boston, MA, 354–355.
- Janjić, Z.I., 1994. The step-mountain eta coordinate model: further developments of the convection, viscous sublayer, and turbulence closure schemes. *Mon. Weather Rev.* 122 (5), 927–945.
- Janjic, Z.I., 2002. Nonsingular implementation of the mellor-yamada level 2.5 scheme in the NCEP meso model. *NCEP Office Note No* 437, 61.
- Kain, J.S., Fritsch, J.M., 1990. A one-dimensional entraining/detraining plume model and its application in convective parameterization. *J. Atmos. Sci.* 47 (23), 2784–2802.
- Kalnay, E., Kanamitsu, M., Kistler, R., et al., 1996. The NCEP/NCAR 40-year reanalysis project[J]. *Bull. Am. Meteorol. Soc.* 77 (3), 437–472.
- Lakhima, C., et al., 2018. Impact of microphysics parameterizations and horizontal resolutions on simulation of “MORA” tropical cyclone over Bay of Bengal using Numerical Weather Prediction Model. *Meteorol. Atmos. Phys.* 1–13.
- Lin, Yu-Hsien, Fang, Ming-Chung, Ronald, W. Yeung, 2013. The optimization of ship weather-routing algorithm based on the composite influence of multi-dynamic elements. *Applied Ocean Research* 43, 184–194.
- Lo, J.C.F., Yang, Z.L., Pielke Sr, R.A., 2008. Assessment of three dynamical climate downscaling methods using the Weather Research and Forecasting (WRF) model. *J. Geophys. Res.: Atmosphere* 113, D9.
- Lu, L.F., et al., 2017. Rough wave simulation and validation using onboard ship motion data in the Southern Hemisphere to enhance ship weather routing. *Ocean Eng.* 144, 61–77.
- Mahala, B.K., Mohanty, P.K., Nayak, B.K., 2015. Impact of microphysics schemes in the simulation of cyclone phailin using WRF model. *Procedia Eng.* 116, 655–662.
- Marelle, L., et al., 2016. Air quality and radiative impacts of Arctic shipping emissions in the summertime in northern Norway: from the local to the regional scale. *Atmos. Chem. Phys.* 16 (4), 2359–2379.
- Mlawer, E.J., Taubman, S.J., Brown, P.D., Iacono, M.J., Clough, S.A., 1997. “Radiative transfer for inhomogeneous atmospheres: RRTM, a validated correlated-k model for the longwave. *J. Geophys. Res.* 102, 16663–16682.
- Mooney, P.A., Mulligan, F.J., Fealy, R., 2011. Comparison of ERA-40, ERA-Interim and NCEP/NCAR reanalysis data with observed surface air temperatures over Ireland. *Int. J. Climatol.* 31 (4), 545–557.
- Nakano, T., Yamashiro, M., Hashimoto, N., et al., 2010. Hindcasting coastal sea surface wind by 4DVAR at typhoon 9918[J]. *J. Japan Soc. Civil Eng. Ser. B2 (Coastal Eng.)* 66 (1), 381–385.
- National Centers for environmental prediction/national weather service/NOAA/US department of Commerce. NCEP FNL operational model global tropospheric analyses, continuing from July 1999. *Res. Data Arch. Natl. Center. Atmosph. Res. Comput. Inform. Sys. Lab.*, 2000
- Politi, N., et al., 2018. Evaluation of the AWR-WRF model configuration at high resolution over the domain of Greece. *Atmos. Res.* 208, 229–245.
- Roiger, A., et al., 2016. Quantifying emerging local anthropogenic emissions in the Arctic region: the ACCESS aircraft campaign experiment. *Bull. Am. Meteorol. Soc.* 1, 441–460, 2016.
- Sasa, K., et al., 2015. Evaluation of ship performance in international maritime transportation using an onboard measurement system-in case of a bulk carrier in international voyages. *Ocean Eng.* 104, 294–309.
- Sasa, K., Takeuchi, K., Chen, C., Faltinsen, O.M., Prpić-Oršić, J., Valčić, M., et al., 2019. Evaluation of speed loss in bulk carriers with actual data from rough sea voyages. *Ocean Eng.* 187, 106162.
- Sen, D., Padhy, C.P., 2015. An approach for development of a ship routing algorithm for application in the North Indian Ocean region. *Appl. Ocean Res.* 50, 173–191.
- Shao, W., Zhou, P., Thong, S.K., 2012. Development of a novel forward dynamic programming method for weather routing. *J. Mar. Sci. Technol.* 17 (2), 239–251.
- Skamarock, W.C., Klemp, J.B., Dudhia, J., Gill, D.O., Barker, D.M., Duda, M.G., Huang, X. Y., Wang, W., Powers, J.G., 2008. A description of the advanced research WRF version 3. NCAR Tech. Note NCAR/TN-475+STR 113. <https://doi.org/10.5065/D68S4MVH>.
- Smith, S.D., 1981. Factors for Adjustment of Wind Speed over Water to a 10-metre Height. BI-R81-3. Bedford Inst. of Ocean. Dartmouth, N. S. p. 29.
- Stauffer, D.R., Seaman, N.L., 1990. Use of four-dimensional data assimilation in a limited-area mesoscale model Part I: experiments with synoptic-scale data. *Mon. Weather Rev.* 118, 1250–1277.
- Takahashi, K., Mezaoui, B., Shoji, R., 2009. On the fuel saving operation for coastal merchant ships using weather routing. *Proc. Int. Symp. TransNav.* 9.
- Vettor, R., Soares, C.G., 2016. Rough weather avoidance effect on the wave climate experienced by oceangoing vessels. *Appl. Ocean Res.* 59, 606–615.
- Vincent, C.L., Hahmann, A.N., 2015. The impact of grid and spectral nudging on the variance of the near-surface wind speed[J]. *J. Appl. Meteorol. Climatol.* 54 (5), 1021–1038.
- Zeyaeayan, S., et al., 2017. Evaluating the effect of physics schemes in WRF simulations of summer rainfall in North West Iran. *Climate* 5 (3), 48.